IRWIN AND JOAN JACOBS
CENTER FOR COMMUNICATION AND INFORMATION TECHNOLOGIES

Automatic Gain Control of Images Motivated by Human Vision

S. Furman and Y.Y. Zeevi

CCIT Report #793
August 2011

DEPARTMENT OF ELECTRICAL ENGINEERING
TECHNION - ISRAEL INSTITUTE OF TECHNOLOGY, HAIFA 32000, ISRAEL

CCIT Report #793 August 2011

Automatic Gain Control of Images Motivated by Human Vision

S. Furman, Y.Y. Zeevi

Abstract— Biologically-motivated Automatic Gain Control (AGC) scheme of processing along various image dimensions is presented. Images are represented in a multidimensional space that incorporates less investigated dimensions such as curvature, size, depth, convexity/concavity and more. Similarly to the effect of AGC on processing of intensity in vision, the proposed scheme for multidimensional image processing and computer vision enhances and emphasizes important image attributes along each dimension of the representation by adaptive nonlinear filtering. This achieves vision-like intelligent image processing and new powerful means for computer vision. The proposed AGC scheme is analyzed for its SNR characteristics, and for its action on several specific inputs. The results are compared with effects known from visual psychophysics, exhibiting reproduction of visual illusions. Finally, examples of applications in computer vision are presented. These include processing of HDR (High Dynamic Range) images, enhanced edge detection and interpolation of curves partly occluded during the acquisition process. Incorporating a generic neural network AGC scheme along all the visual dimensions, constitutes a universal, parsimonious and unified model that can span a multidimensional HDR, and yet be sensitive to fine details along all the dimensions. Implementation of the multidimensional AGC in image processing and computer vision may also contribute to the development of a metric for image space, and facilitate further development of new means for recognition and classification.

Index Terms—Computer vision, Computational models of vision, Filtering Enhancement, Projections, Multidimensional Image Representation, Size and shape, Depth cues, Neural nets Models.

1 Introduction

THE perceived image is quite different from the original image projected onto the retina. Some of the image features that are of great importance (biologically speaking) are enhanced, whereas other that are not significant are barely noticed or even ignored (i.e. suppressed). Many examples of this selective enhancement/suppression phenomenon exist. Usually they are referred to as "visual illusions" (See Fig. 1 for such examples), but all of them can be explained by the way the human visual system (HVS) generally processes visual information, implementing non-linear AGC mechanisms.

Understanding the organization and functioning of visual systems is obviously of great interest and importance in the field of image processing and computer vision because of its potential use in the design of intelligent systems that mimic biological vision (for such examples see [1] [2]). By matching image presentations to the known performance of the visual system, more meaningful and efficient communication can be achieved. After all, most of information generated for human consumption, is communicated with the human observer via the visual system as the final receiver. In yet another way, image processing modeled after the visual system may prove to be important in machine (computer) vision. And of course, now that visual prosthetics are becoming a workable reality [3], this understanding is essential. Moreover, such an understanding may lead to the development of an image metric accounting for human perception. This should contribute to further advancement of recognition and classification algorithms.

Each cone in the central fovea is connected to about 4000 cortical neurons [4]. The challenge to determine what are these 4000 processes, and what are the structure and function of this multidimensional representation, still remains outstanding.

Orientation and ocular dominance (OD) [5] can account for 40 different processing units (20 different orientations for each ocular projection). This leaves an unexplained factor of 4000/40=100! There are several candidates for the remaining functions, such as color, intensity, texture, curvature, range of field sizes and binocular disparity (for depth perception).

Gibson [6] had claimed that adaptation and negative after-effect are to be conceived as a process of adjustment and readjustment of the physical-phenomenal correspondence of a certain type of sensory dimension, under the influence of a tendency for sensory activity to become normal, standard or neutral. He noticed that this similarity cuts across the sensory modalities of our world, including pressure, size, distance, temperature, brightness, curvature (convex-concave), etc.

Zeevi & Mangoubi [7] showed that Adaptation plays an important role in the suppression of quantal and receptor internal noise. Wainwright [8] proposed that visual adaptation in orientation, spatial frequency, and motion can be understood from the perspective of optimal information transmission. Ullman [9] had claimed that adaptation and gain control can fulfill two useful functions: correction of errors and recalibration. In multi-channel mode (i.e. in the spatial case), the gain control helps to maintain the overall sensitivity of the system: if the gain of one of the channels increases, the gain of neighboring channels decrease, and vice versa.

Automatic Gain Control (AGC) has been widely used to account for many sensory adaptations. Shefer used it for intensity adaptation [10], Weltsch for contrast adaptation in the primary visual cortex [11], Sperling for contrast adaptation for "cyclopean" image [12] and for contrast adaptation for motion detection [13], Du Croz and Krauskopf for chromatic adaptation [14] and [15], Shapley for retina adaptation [16] and Schwartz for sound adaptation [17]. It is, therefore natural and tempting to implement the AGC model in processing images which incorporate some other less investigated dimensions of adaptation, such as size, depth and curvature, in processing of images. Likewise, such an investigation may facilitate our understanding of how adaptation along these dimensions takes place in the visual system (or other sensory modalities for this matter).

The purpose of this study is to analyze adaptation along less investigated image dimensions and process these image attributes by means of the AGC model in order to mimic the human visual system (HVS), and to propose a unified framework for sensory information processing. Such a framework considered in the context of vision (biological and computer-based alike), can be also implemented in advanced image processing algorithms that highlight various features and image structures. Such a multidimensional adaptive framework of image processing, can then be implemented in intelligent image processing and computer vision systems, similarly to the high dynamic range camera that mimics the eye [18], [19], that has become the gold standard of cameras and other image acquisition systems. The performance of the proposed multidimensional AGC framework of image processing is tested by computer simulations, for each dimension separately, and

is compared to the results of psychophysical experiments.

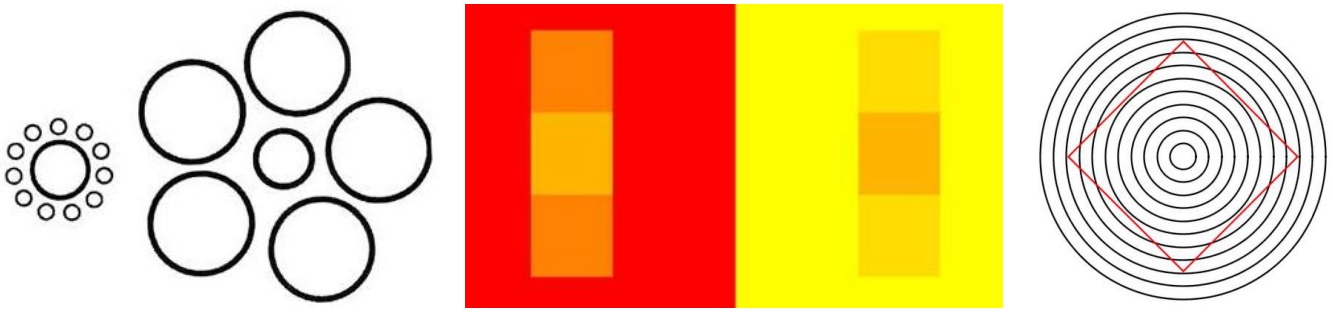

(a) (b) (c)

Fig. 1: Effects of size (a), color (b) and curvature (c) contrast. (a) Both circles in the middle are of the same size. (b) Both squares in the middle are of the same color. (c) The square's boundaries are straight lines, but they are perceived as being curved.

2 THE BASICS OF VISUAL AGC FRAMEWORK

THE proposed AGC model of visual adaptation is based on the original work of Shefer and Zeevi [10], and on the subsequent development of the adaptive sensitivity camera that mimics the eye [18], [19]. The model has been motivated by the structure and function of the retina and, in particular, by its high spatio-temporal sensitivity to small changes in intensity accomplished over extremely wide dynamic range. According to this nonlinear AGC adaptation model, the output of a biological or artificial visual sensory cell (i.e. detector) is adjusted by subtracting from its input a nonlinear function of its input and a feedback signal, which is a local weighted sum of the outputs (Fig. 2):

$$r_i = \alpha \cdot s_i - \mathrm{T}(s_i, f_i), \qquad (1)$$

where r_i is the output (or response) of cell i, s_i is the input (W in Fig. 2 is the weighting of a feedback operator (matrix)), f_i is the feedback (see (3)), α is a constant and T is a nonlinear input-output-feedback interaction function. The crucial ingredient of this AGC model is the nonlinearity within the local feedback loop (i.e. the function T). This is a fundamental extension of the lateral inhibition (i.e. linear output convolution) feedback model into the nonlinear regime, presumed to be biologically mediated by the retinal interplexiform cells and/or similar structures in other loci along the processing pathway, and/or other sensory networks. It is important to note that qualitatively T may assume a wide range of nonlinear functions and, yet, the feedback loop in which such nonlinear function is embedded will exhibit functional AGC (see [20] and [21] for such examples).

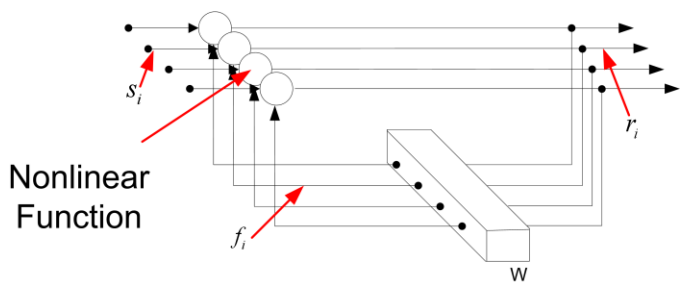

Fig. 2: The core of AGC sensory adaptation model.

If we assume that the cells (pixels processing units) are small and close enough, we can model the feedback operator by a continues function, and use convolution to represent the W action on the output. Extending the proposed AGC framework to other image dimensions, each of the functions of x is a dependent variable that stands for curvature, size, depth etc. In this case, (1) is written as:

$$r(x) = \alpha \cdot s(x) - \mathrm{T}(s(x), f(x)). \quad (2)$$

In a specific embodiment of this general conceptual model, the nonlinearly component is a multiplier (Fig. 3). The model is then comprised of a series of static instantaneous multipliers, one for each foveal receptor channel, that multiply the input of the channel with the output of the feedback. The feedback is calculated by subtracting the output of the local operator W from a constant value. The operator W is a local averaging operator (in space).

The feedback $f(x)$ is obtained by a convolution of W with the output $r(x)$:

$$f(x) = \int r(x')W(x-x')dx'. \quad (3)$$

The AGC model output (derived from (2)) is given by:

$$r(x) = s(x)\left[\alpha - \left|\int r(x')W(x-x')dx'\right|\right]. \quad (4)$$

The function of the feedback is to position the enhancement mechanism, high gain operating curve, symmetrically around the local operating point. W can be chosen as exponent, gaussian, triangle, rectangular or any other symmetric kernel for which one can obtain the qualitative characteristics of the AGC. The quantitative behavior will, of course, depend on the specific choice of W.

The operator, i.e. image processor (4) has a unique solution for

$$\max_x\{|s(x)|\} < 1/S_W, \quad (5)$$

where S_W is:

$$S_W = \int W(x)dx. \quad (6)$$

These conditions can be extended using the discrete form of W:

$$w_i > 1; \quad \sum_{j\neq i}|w_j| < 1 \quad (7)$$

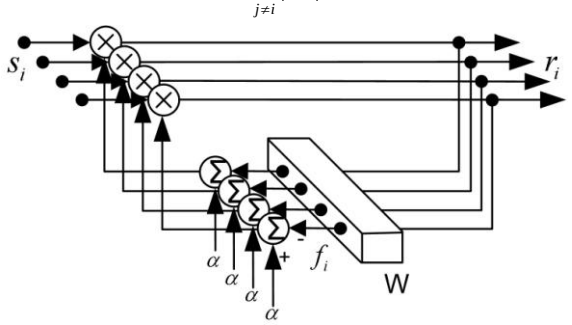

Fig. 3: Schematic diagram of a specific embodiment of the generic AGC processor, where the nonlinear interac-

tion in the feedback loop is implemented by a multiplier.

2.1 Small Signal Analysis

Although we are concerned in general with "large signal" performance of the visual AGC, it is nevertheless useful to perform also small signal analysis of the model. However, we note that the case of small signal is also of interest physically. Considering the wide dynamic range of intensity to which the visual system (or any image acquisition system) is exposed, at any specific time and/or position the intensity varies only over a relatively narrow range of intensities. For the small signal analysis we assume that both the output and the input of the model are comprised of a 'local DC' modulated by a small AC signal component:

$$\tilde{S}(x) = C_s + s(x);\quad \tilde{R}(x) = C_r + r(x)\,, \tag{8}$$

$$\int s(x)dx = 0;\qquad \int r(x)dx = 0\,. \tag{9}$$

For simplicity, we assume also that W is a rectangular function. Under these assumptions, (3) yields:

$$f(x) = \int_{\Omega} \tilde{R}(x')W(x-x')dx' = \int_{\Omega} \tilde{R}(x')dx' = C_r\,, \tag{10}$$

where Ω is the integration region, limited by the width of W.

Substituting (8), (9) and (10) for the corresponding variables in (4) yields, one obtains:

$$r(x) = s(x)\frac{\alpha}{1+C_s}\,;C_r = \frac{\alpha \cdot C_s}{1+C_s}\,. \tag{11}$$

Equation (11) expresses a sigmoidal function for the AC response, which is closely related to Weber law of sensory perception. The latter implies that the system gain is inversely proportional to the input's local DC. Examining the local DC response (C_r) reveals a highly compressive response curve that never exceeds the value of "1" (see Fig. 4 – black line). This means that the system has theoretically unlimited dynamic range, and yet, for each local DC value, the system exhibits high sensitivity (see Fig. 4 – red lines depicting a sequence of AC response curves for various values of local DC).

Weber law is characteristic of many sensory modalities, including weight, vision, touch and sound.

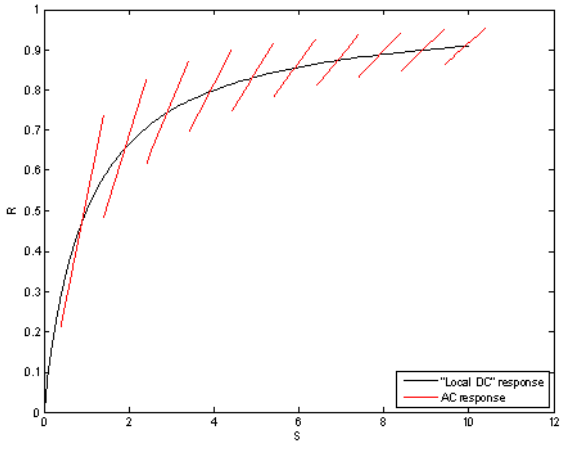

Fig. 4: Small signal response. The AC, r(x), (in red), is shown superimposed on the "local DC", C_r, response (in black).

2.2 Simulations

In its discrete form, (4) exhibits the complexity of a manybody problem. To obtain a closed form solution for some arbitrary input is a major challenge, not yet dealt with. Therefore, we employ a numeric solution of an iterative process. Fig. 5 presents the flow chart of the algorithm for numeric solution of the AGC model.

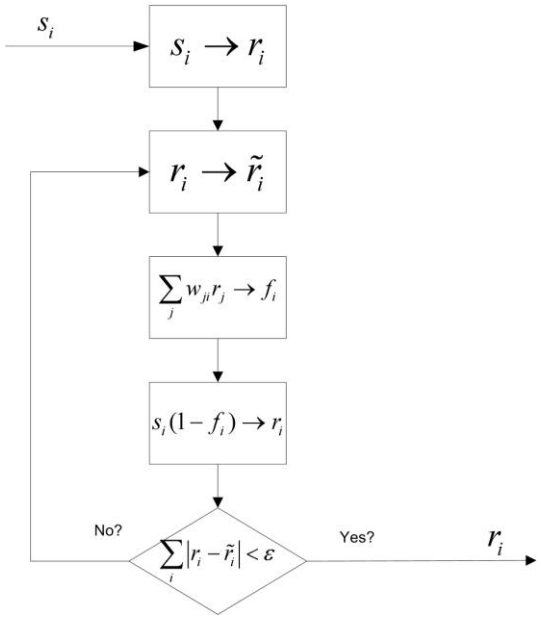

Fig. 5: Flowchart for calcuating the visual AGC response to some arbitrary input.

The solution is unique, provided the process converges [10].

2.3 Step Response

We now explore two of the main functional features of the models – adaptation and edge enhancement, by examining the step/ramp response of the models. The step/ramp response is of special interest, since steps occur in natural stimuli [22], and are often used to study the dynamics of adaptation. Fig. 6 depicts step response of the non-linear AGC model, superimposed on the step. This example highlights the main characteristics of the model:

Adaptation: The response adapted to a constant input is decreased, while high values are more affected than lower values. This is, in a way, compression of a wide dynamic range of the input.

An edge enhancement: the relative contrast is increased. This is caused by the overshoot and undershoot of the model response. Note that due to the nonlinearity of the model, the overshoot is stronger than the undershoot, and both of them are depended on the slope of the input step (Fig. 7). When the input represents intensity, this phenomenon is well known as "Mach Bands" [23].

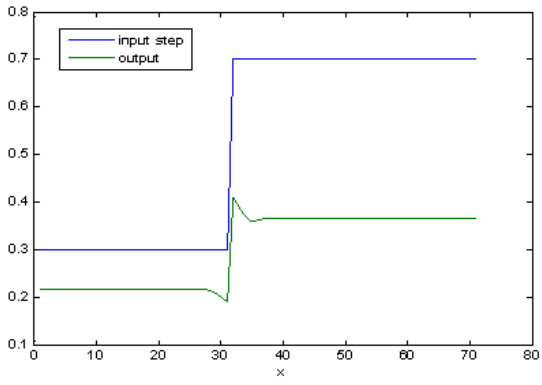

Fig. 6: Step response of the AGC model, superimposed on a step stimulus.

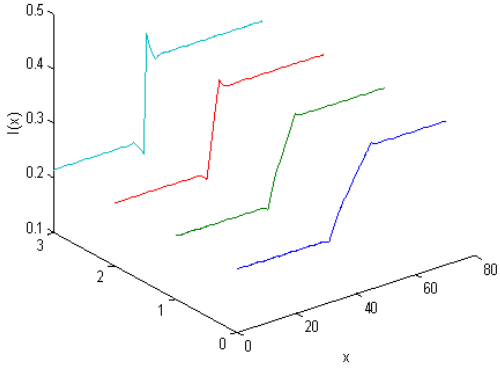

Fig. 7: AGC model responses to various input slopes.

2.4 Noise and SNR Analysis

Various types of noise are encounted in vision and imaging systems, e.g. the quantal noise and the neural noise (for more details see [24]), or imaging detector noise. We assume that the noise is additive, has zero mean and small variance σ_s^2 compared with the signal:

$$S_n(x) = s(x) + \eta_s(x), \tag{12}$$

where $s(x)$ is the noise-free input, $\eta_s(x)$ the noise of the source (input), and $S_n(x)$ is the noisy input.

We are mainly concerned in the context of the noise and SNR analysis with input that is locally constant. In other words, we consider here areas but with only gradual changes of the input and no sharp edges. We do not deal with the edges for two reasons: first, edges constitute only a small part of the image, i.e. most of the image pixels belong to areas that are characterized by being locally constant. Second, if an edge is sharp, it isn't affected by the noise.

Observing the similarity of (12) and (8), suggests that we may analyze the effect of the noise using the same analysis employed in the case of the small signal, where the input signal is analogous to C_s, and the noise is analogous to $s(x)$. In the latter case, the output noise is:

$$\eta_r(x) = \eta_s(x)\frac{\alpha}{1+s(x)}. \tag{13}$$

Equation (13) implies that the average and variance of the response noise are:

$$\mu_r = \frac{\alpha}{1+s(x)}\mu_s = 0; \qquad \sigma_r{}^2 = \left(\frac{\alpha}{1+s(x)}\right)^2 \sigma_s{}^2, \tag{14}$$

whereas (14) implies that the output noise variance depends on the input signal. It depicts noise suppression as a function of the input intensity, consistent with measurements and psychophysical results (see [7] and [25] for more details).

Note that the above analysis does not postulate any assumptions regarding the noise characteristics (such as independency and/or distribution) besides small signal assumption.

Another way to evaluate the noise variance at the output is as a function of a random variable [26]:

$$\sigma_r{}^2 \cong \left[g'\left(\bar{\eta}_s\right)\right]^2 \sigma_s{}^2, \tag{15}$$

where $r = g(s)$ is a smooth function of s, $\sigma_r{}^2$ is the variance of the response, $\sigma_s{}^2$ is the variance of the input, and $\bar{\eta}_s$ is the average of the input. In the case of additive noise, the input can be written as in (12), implying that the input consists of a noise-free component $s(x)$ and noise with a zero mean. However, since we deal with an implicit equation (see (4)), calculating its derivative is not feasible. We therefore obtain an explicit form by using the discrete form, yielding the response of cell i is a function of the input to this cell, and the responses of the other cells (see (17)). Therefore:

$$\sigma_{r_i}{}^2 \cong \left[g'\left(\bar{\eta}_{s_i}\right)\right]^2 \sigma_{s_i}{}^2, \tag{16}$$

$$r_i = g\left(s_i\right) = \frac{s_i(\alpha - \sum_{j\neq i} w_j r_j)}{1+s_i w_i}, \tag{17}$$

$$g'\left(s_i\right) = \frac{\partial r_i}{\partial s_i} = \frac{(\alpha - \sum_{j\neq i} w_j r_j)\left(1+s_i w_i\right) - s_i w_i(\alpha - \sum_{j\neq i} w_j r_j)}{\left(1+s_i w_i\right)^2} = \frac{(\alpha - \sum_{j\neq i} w_j r_j)}{\left(1+s_i w_i\right)^2}. \tag{18}$$

Assuming that $g\left(s\right)$ is a smooth function of s, the variance is:

$$\sigma_{r_i}{}^2 \cong \left[\frac{(\alpha - \sum_{j\neq i} w_j r_j)}{\left(1+\bar{\eta}_{s_i} w_i\right)^2}\right]^2 \sigma_{s_i}{}^2. \tag{19}$$

Equation (19) shows, again, that the response variance is inversely proportional to the input average $\bar{\eta}_{s_i}$.

Note that this analysis does not necessitate any restrictive assumptions regarding noise characteristics. Only the first two moments are required.

We can define the SNR characteristics of the system as:

$$SNR = \frac{signal^2}{\sigma^2} = \frac{\tilde{C}_m{}^2}{\sigma^2}, \tag{20}$$

where $\tilde{C}_m$ is the Michelson contrast:

$$\tilde{C}_m = \frac{I_{\max} - I_{\min}}{I_{\max} + I_{\min}}. \tag{21}$$

$I_{\max}$ and $I_{\min}$ being the highest and the lowest intensity values respectively. Note that in the case of the response, the cal-

culated maximum and minimum values include the overshoot and undershoot.

For a general step input (i.e. sharp, on-dimensional edge in the case of an image),

$$s(x) = a_1 + a_2 U(x), \tag{22}$$

where a_1 is the lower constant value (intensity) of the step and $a_1 + a_2$ is the upper constant (intensity) value, the SNR is improved by:

$$\frac{SNR_r}{SNR_s} = \left(\frac{1+a_1+a_2}{\alpha}\right)^2 \; or \; \left(\frac{1+a_1}{\alpha}\right)^2, \tag{23}$$

where the two alternative measures of SNR noise improvement options are related to the noise at the upper part or lower part (left) of the step (edge), respectively. It is interesting to observe that the SNR improvement is equal exactly to the noise suppression factor of the AGC model. This is due to the fact that the contrast of the input signal is equal to the contrast of the response [See Appendix A for more details].

3 AGC MODEL/ALGORITHM IMPLEMENTATION ALONG CURVATURE/SIZE/DEPTH AND CONVEX-CONCAVE DIMENSIONS

3.1 Background

3.1.1 Overview of Differential Geometry

To establish the context in which curvature processing is formulated, it is useful to review a few elementary notions adopted from differential geometry The review is focused on curves in the plane, but the results can be generalized to higher dimensional (see, for example, [27] for more details).

Let I be an interval in one-dimensional Euclidian space E^1. A curve C is defined as a continuous mapping $x: I \to E^2$ from the interval to the plane, where

$$x(\lambda) = (x_1(\lambda), x_2(\lambda)). \tag{24}$$

A curve may be reparameterized in terms of its arc length s:

$$x(s) = (x_1(s), x_2(s)). \tag{25}$$

The curvature κ is then defined as rate of change of orientation per unit arc length:

$$x''(s) = (x_1''(s), x_2''(s)) = \kappa n \qquad or \qquad \kappa = \frac{x_1'(\lambda)x_2''(\lambda) - x_1''(\lambda)x_2'(\lambda)}{(x_1'(\lambda)^2 + x_2'(\lambda)^2)^{3/2}}, \tag{26}$$

while the geometric interpretation for the curvature is the curve radius:

$$rad = \frac{1}{\kappa}. \tag{27}$$

3.1.2 Locality and parallelism of curvature, size and depth

A key fact regarding the structural and functional organization of the HVS (which supports our AGC model and serves as the basis of our image representation and processing algorithm) is that processing along image dimensions of size, curvature, depth and/or other dimensions is performed locally and in parallel over the entire image [28]. These image dimen-

sions are believed to correspond to "Elementary Features" [29], [30] of image representation in the HVS. Consequently, the image is decomposed along a number of dimensions and into a number of separable components.

This concept had been tested in many psychophysical experiments such as “pop-up” experiments. In these experiments, there is a target with a unique feature which is not shared by the distractors. If the feature is detected early along the visual pathway, and if visual processing is performed locally and in parallel, the target should “pop-up” from the distractors with little effect of the number of distractors. Treisman & Gormican [31] showed that such "pop-up"s are asymmetric in that some features are detected more easily when they are present rather than when they are absent, which implies that the processing is non-linear. Fig. 8 presents an example of such experiment for target defined by convexity/concavity depth cues (See [32], [33]).

We may conclude that size, curvature and depth are processed locally and in parallel.

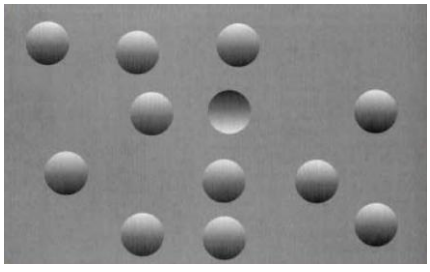

Fig. 8: An example of a display, used in testing search for targets defined by depth cues. The target “pops-up” from the distractors with little effect of the number of distractors.

3.1.3 Adaptation and feature detectors

It is well known that prolonged inspection of a curved line causes adaptation to curvature (e.g. the curvature after-effect [6], [34]). Such after-effects are believed to reflect a change in the sensitivity of neurons that encode the adapted feature and, thus, imply the existence of neurons that act as detectors of that feature [35].

Indeed, most of the investigators agree that curvature detectors are present along the early stages of the visual pathway [36], [37]. Some investigators have shown how such curvature calculations can be obtained by convolution with certain reasonable receptive fields of neural cells [38], [39]. Wilson et al. have shown how global curvature information can be extracted from local detectors using concentric glass patterns [40].

Sutherland [41] concluded that many species have the capacity to classify a shape as the same shape regardless of changes in size, at least over a considerable range, and that this capacity is innate. This ability can be addressed as irrelevance of the DC component of size information (adaptation) and relevance of changes only.

Blakemore and Campbell [42] suggested that the human visual system may possess neurons selectively sensitive to size. They also hypothesized that this neural system may play an essential preliminary role in the recognition of complex images. Carey et al [43] suggested that size, motion and orientation measures are processed in parallel by the dorsal

stream mechanisms.

The visual system perceives depth based on several cues such as stereoscopic views, motion-parallax, object size, object translation and rotation. Hubel and Wiesel, [44] have identified cells that are involved in depth information representation from stereoscopic vision. A number of authors have reported simultaneous depth contrast effects for stimuli defined by stereoscopic, motion parallax and other (see [45] and [46]).

Existence of adaptation and contrast effect of a specific feature is closely related to existence of detectors of this feature (or a specific channel). Adaptation and contrast effects are well documented with reference to curvature, size and depth. It, therefore, seems reasonable to assume that curvature, size and depth information are processed over the entire image (in parallel), by neural structures wherein each cell (or group of cells) corresponding to a specific location represents local feature information.

3.1.4 Retinotopic mapping concept

This concept was first introduced by Hubel and Wiesel [47] within the context of retinotopic representation. We recall this concept to conclude the findings outlined in the last two sections. We actually expend this concept and apply it to all image dimensions (curvature, size, depth, color, etc.), and assume that the HVS consist of multiple networks of cells that create multiple projections along image dimensions, wherein neighboring regions of the cells preserve the neighborhood regions of the feature in the image. Fig. 9 depicts this generalized concept. The HVS consists of multiple networks, one for each image dimension – size, color, curvature etc. Each network consists of many feature detectors. Each detector is a location specific. Together these detectors cover the entire image, and form a network that projects the image along a specific dimension.

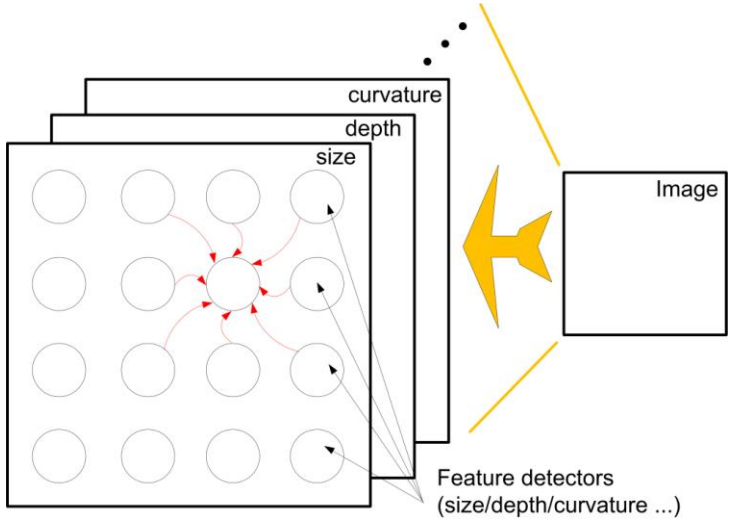

Fig. 9: The retinotopic mapping concept: The HVS consists of multiple networks of cells that create multiple projections along image dimensions, wherein neighboring regions of the image are preserved by neighboring regions of the visual map.

Based on the above reasoning, it is natural to assume that these networks exhibit AGC characteristics. Therefore each image dimension processing in vision (or other sensory modalities for this matter) can be modeled by an AGC system.

3.2 Psychophysical Experiments

Two psychophysical experiments are presented as examples. The first is the size contrast effect (the Ebbinghaus illusion), while the second is concerned with the depth contrast effect. The AGC model/algorithm reproduces the illusions.

3.2.1 Size Contrast

The Ebbinghaus illusion is commonly used as an example of a simple size-contrast effect. In this illusion, the apparent size of a central target is affected by a ring of surrounding inducers. Fig. 1(a) illustrates a well-known form of this illusion, as it most often appears in general textbooks. This form is typically used to illustrate a simple size-contrast effect, in which large inducers make the target appear smaller while small inducers make it appear larger.

Roberts et al [48] have further investigated the above effect and concluded that it arises from a number of factors that include the relative size of the inducers (comparing to the target), the number of inducers, and their distance from the target. These authors found that the apparent size of the target is reduced more efficiently when the inducers get bigger and at larger distances (see Fig. 10).

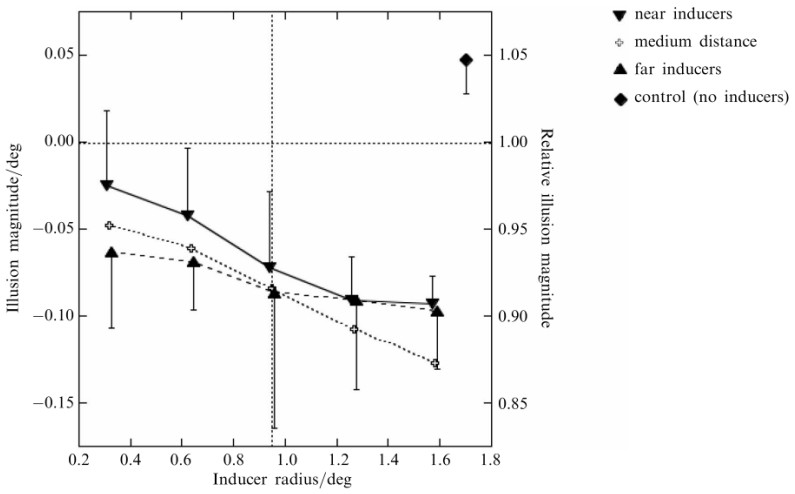

Fig. 10: Results of the Ebbinghaus illusion experiment (adopted from [48]) showing that apparent size of the target is reduced as the inducers get bigger, consistent with a size-contrast effect. The effect is emphasized when the inducers are at larger distances.

3.2.2 Depth Contrast

Graham and Rogers [46] have shown depth-contrast effect perceived from motion parallax and stereoscopic information. The perceived effect is illustrated in Fig. 11. The perceived depth is affected by the surrounding, and so, even though bar A and bar B are at the same physical depth, they are perceived as though bar A is in front of bar B.

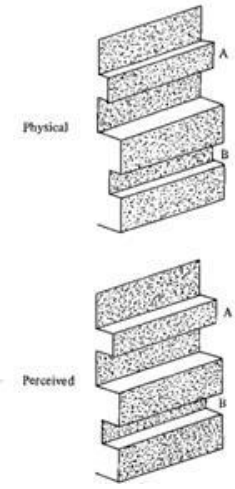

Fig. 11: Depth-contrast effect (adopted from [46]): bar A is perceived as lying in front of bar B, although they are physically at the same depth.

3.3 Simulation Results

We assume that visual information is represented in a multidimensional image space, but are not concerned with the issue of how this information was extracted, or projected onto this space. This assumption is reasonable, since many techniques of depth/size/curvature (or other image dimensions) estimation are available. [For an example of a technique for curve estimation see [49] and [50].]

3.3.1 Curvature Processing

In this section two curves are presented. The first one is a curve with constant curvature, i.e. a section of a circle (Fig. 12). The second is a combination of straight lines and sectors of circles with an opposite curvature (Fig. 13).

The AGC parameters used in the processing of both curves are: $W(x) = k\frac{\gamma}{2}e^{-\gamma|x|}; k = 20; \gamma = 0.2$, with W extending across 5 pixels.

The first result depicts curvature adaptation – the curvature is decreased, whereas the second result highlights curvature enhancement (or emphasis). For presentation and comparison purposes, only, the curvature result of the second curve is multiplied by a factor 1.87, to "compensate" for the adaptation phenomenon and highlight only the curvature enhancement phenomenon. Red circles have been added to Fig. 13 to emphasize the changes between the original curve, and the result. Points that are inside the circles have larger curvature than points that are on the circle. Therefore, the edge points (where a change in the curvature occurs) are emphasized in the same way as at Fig. 6.

(a) (b)

Fig. 12: Results of AGC processing of constant curvature, representing spatial adaptation along the curvature dimension. (a) is the original curve (i.e. the input to the system) and (b) is the result of (a) being processed by the AGC algorithm (i.e. the response of the model).

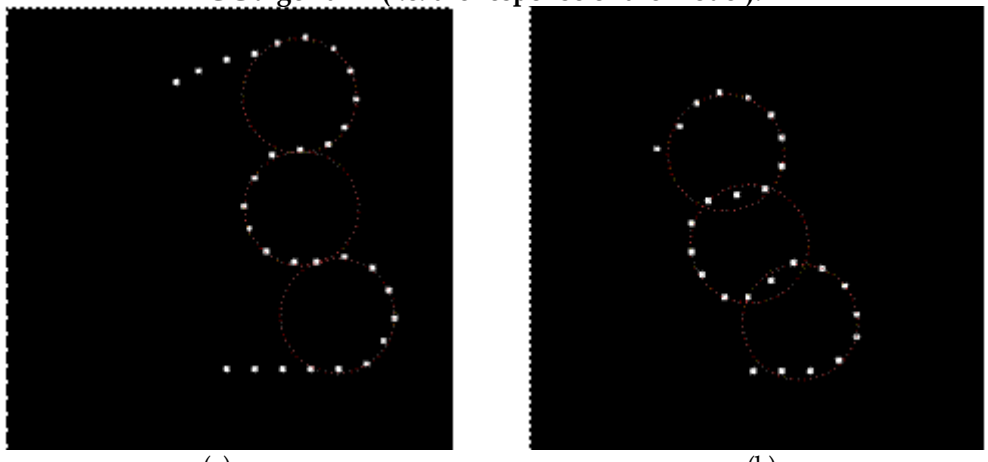

(a) (b)

Fig. 13: Results of AGC processing of fragmented curvature curve representing edge enhancement along the curvature dimension. (a) is the original curve (i.e. the input to the system) and (b) is the result of (a) being processed by the AGC algorithm.

3.3.2 Curvature Noise

Fig. 14 and Fig. 15 demonstrate the effect of noise, and noise suppression along the curvature dimension.

Comparing the noisy curves' traces with their traces after curvature AGC processing reveals noise suppression that monotonically increases with the magnitude. This is consistent with the above SNR analysis. Note that the noise is suppressed over the curved parts, while it is not affected where there is zero curvature (i.e. the input value has magnitude of zero), (Fig. 15).

3.3.3 Size Processing

To highlight the effect of AGC on size processing, we reconstruct the Ebbinghaus illusion experiment [48], simulating the perceived target size by the AGC algorithm using parameters of: $W(x) = k(\frac{2}{121} - \gamma|x|)\, when: k = 5, \gamma = 0.00007$. These parameters correspond to a lateral effect of a triangular W function with width of 121 image elements (pixels).

The setup of the psychophysical experiment was reproduced. Target was surrounded by 8 inducers at different radii (varying from 5 to 20 pixels). This was checked for near, medium and far (30, 40 and 50 pixels away from target, respectively) inducers. Target radius was 10 pixels. Target size (in pixels) as a function of inducer radius and distance is shown

in Fig. 16. The AGC-processed results are consistent with the original experimental results.

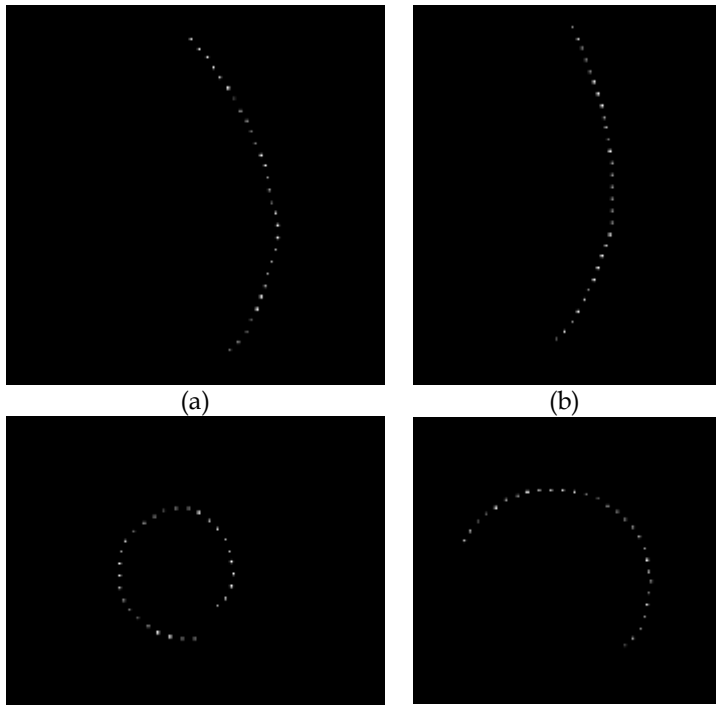

Fig. 14: The effect of noise and noise suppression demonstrated on a curve with constant curvature. (a) and (c) are curves with a constant curvature of 0.2 and 0.7 respectively, with additive Gaussian noise. (b) and (d) are the results of (a) and (c) processed by the AGC algorithm, respectively. The noise suppression, characteristic of this processing, increases with the magnitude (i.e. the curvature) of the input.

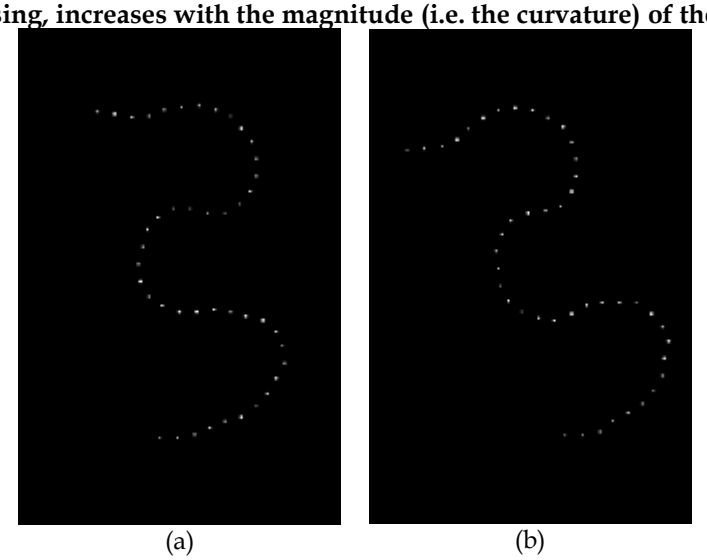

Fig. 15: Noise suppression demonstrated on noisy fragmented curve. (a) A fragmented curve of negative, -0.8, and positive, 0.8, curvature with additive Gaussian noise. (b) The result of (a) processed by the AGC algorithm. The noise is suppressed when the curvature is different than zero

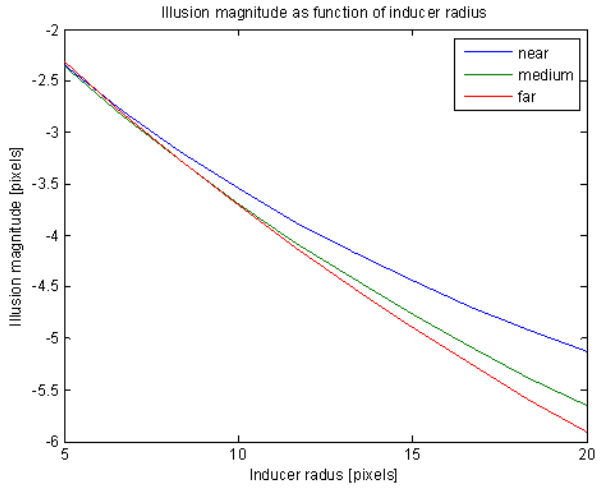

Fig. 16: Results of reproduction of Ebbinghaus experiment using the AGC algorithm. Varying the relative size and distance of the inducers produces changes in the apparent size of the target, consistent with the original experimental results.

It is clear why increasing the inducer size decreases the target perceived size - this represents the size contrast effect of the model. It is less obvious why farther positioned inducers have stronger effect on target perceived size, than that of the closer inducers (i.e. decreasing the target size more effectively). The latter can be understood in the context of the AGC model by W's effective width due to the mutual relation between the inducers. According to the model of AGC visual processing, the impact of cells on their neighbors is limited by W. If the distance between cells is larger compared with W's effective width, then those cells will have a minimum effect on each other (if any). When an inducer is at a given distance x from the target, its distance from the other inducers varies from 0 to $2x$. Thus, when distance increases, more and more inducers are beyond the 'influence zone' of the other inducers. This causes the perceived size of each inducer to increase when the distance is increased. Fig. 17 shows this phenomenon. Since the target is still inside the 'influence zone' of the inducers, and the size of the inducers is now larger, the target seems smaller (the size-contrast effect is enhanced).

Note that here we modeled only the target and inducers as objects with size. But, it is also possible that the visual system treats the space between the target and the inducers as an object with size. In this case, if the space between the target and the inducer is large, the inducer size has only a secondary effect, and the target size is determined mainly by the nearest object (for example see Fig. 18 - Delboeuf illusion. In this illusion, the target gets smaller when the inducer diameter increases). This model can explain also the moon size illusion, as well as other illusions. Likewise, in its implementation in computer vision, the distance between the target and the inducer can be implemented and affect the end result.

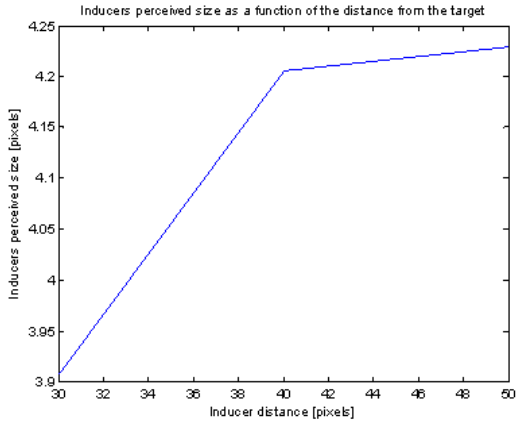

Fig. 17: Results indicating that inducers' perceived size is increased at larger distances. See text for more details.

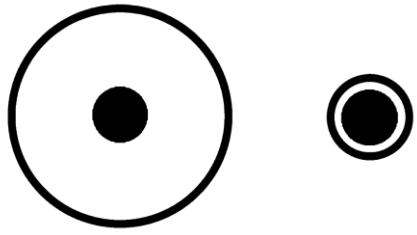

Fig. 18: Delboeuf illusion. The right circle is perceived larger than the left one although they are of the same size.

3.3.4 Depth Processing

To demonstrate the effects of AGC on depth processing, we reproduce the experiment of Graham and Rogers's [46] implementing the visual AGC model, along the visual dimension of depth using the following spatial interaction parameters $W(x) = k\frac{\gamma}{2}e^{-\gamma|x|}; k = 1; \gamma = 0.2$, where the spatial interactions extend across 11 elements.

For each point of the 3D original image the depth is calculated relative to a point in the middle of the image and with height of 50 pixels. Fig. 19 depicts the results in both 3D and cross sections. As a result of the processing by means of AGC, the left bar, which is at the same depth as the right bar, is now perceived closer.

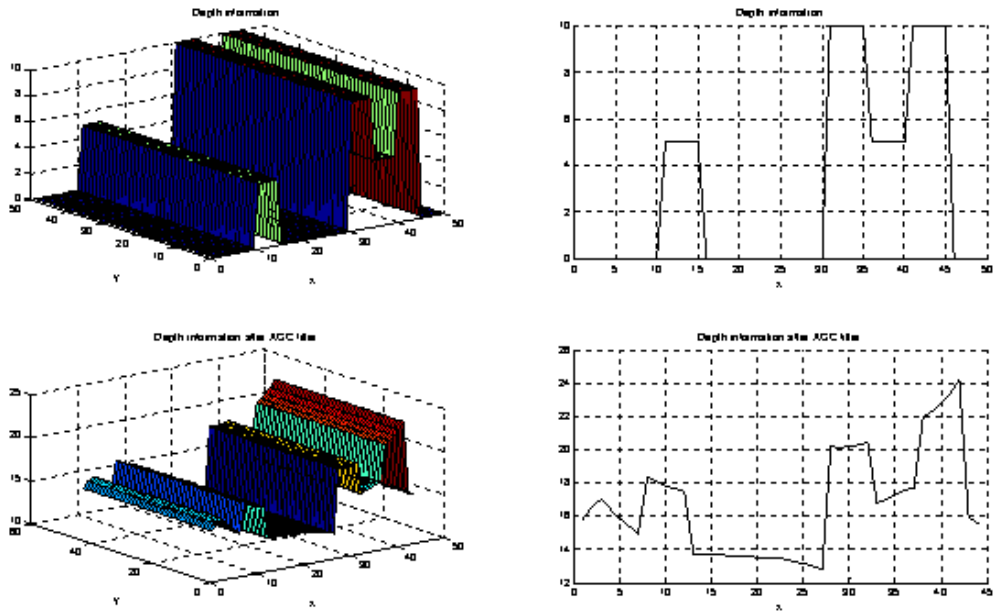

Fig. 19: AGC processing of depth information. Input and output of visual signals are displayed in the top and bottom rows, respectively. The left column is a 3D view, whereas the right column is a cross sections view. Examine the right column - the left bar is perceived as lying in front of the right bar (lower right figure), although they are physically at the same depth (upper right figure). This AGC-processed result is consistent with that of the original depth experiment.

3.3.5 Convex-Concave (2-D curvature processing)

We can take the curvature processing one step farther toward a convex-concave (three dimensional curvature) processing. For that, we generalize the 1-D curvature adaptation of a line into a 2-D curvature adaptation of a 3-D surface. Assuming that the surface does not fold on itself, we can consider it as a function of x and y f(x,y). We can then calculate its x-curvature (along x-z plane) and y-curvature (along y-z plane), comparing to the 1-D curvature (along x-y plane). Consequently, each point of the surface is represented by 2 values (i.e. x and y-curvature) that define the 3-D structure of the surface. The surface structure can be extracted from the curvature values similarly to the 1-D case.

Fig. 20 depicts the results in both 3D and cross section views of AGC convex-concave processing of a similar surface as at the depth processing simulation above. As a result of the AGC processing (right column of Fig. 20), Convexity and concavity are enhanced compared with the original input (left column of Fig. 20). Moreover, points that were originally at the same depth (as the left and right bars in the depth experiment above), are now perceived at different depths, consistent with depth processing results.

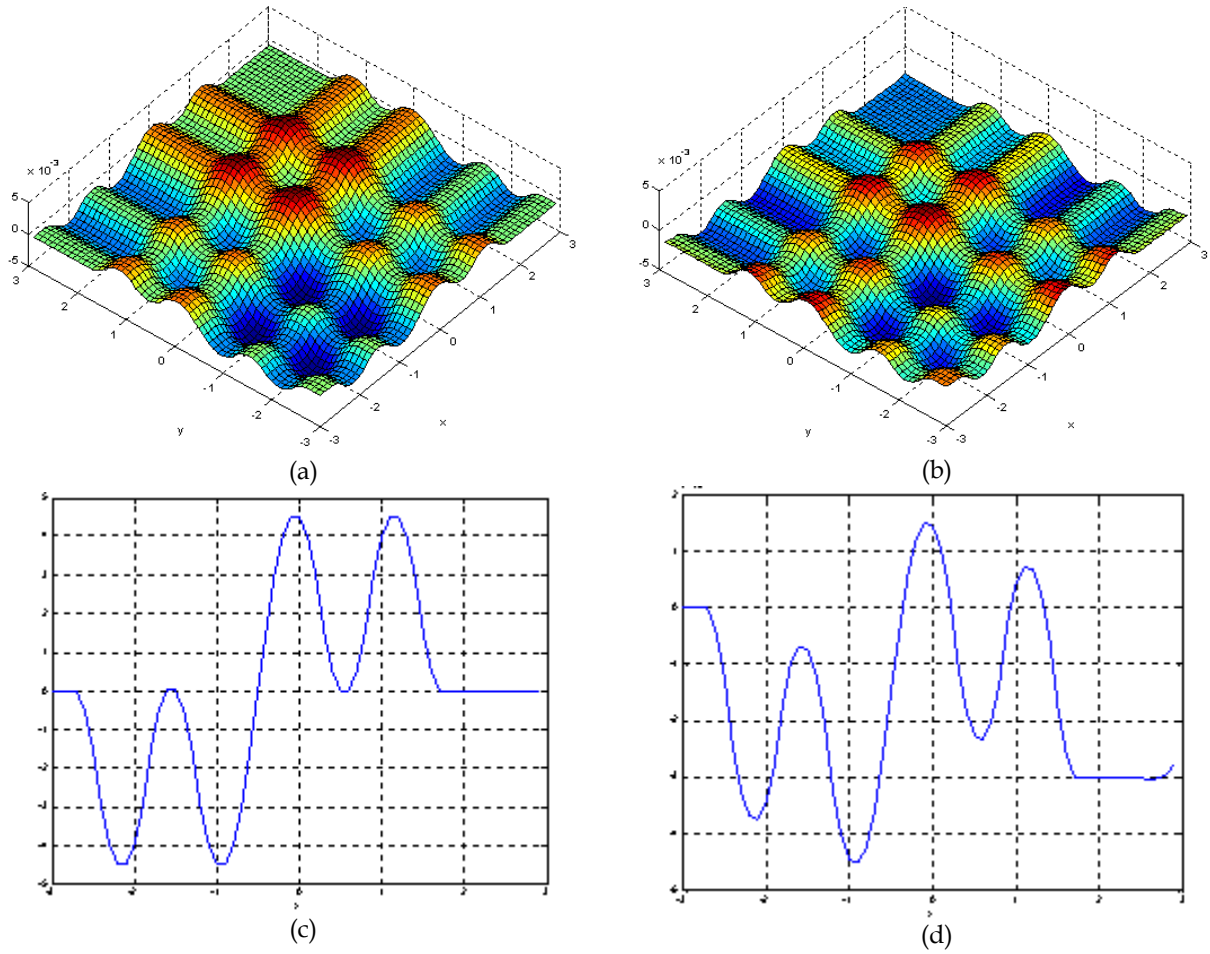

Fig. 20: AGC processing of convex/concave information. (a) is the visual signal input. (b) is the response. Convexity and concavity are enhanced, as can be seen clearly from the cross section views (c) and (d) along the diagonal of the input and response respectively. Moreover, examining the right column - the left bar is perceived as lying in front of the right bar, but they are physically at the same depth (left column). This is consistent with depth processing results (see Fig. 19 for comparison).

4 Applications

THREE applications of AGC-based image/visual processing are presented as examples. Two of them are along the intensity dimension and the third is along the curvature dimension. Note that by all means, these are not the only possibilities, and should be only regarded as examples.

4.1 High Dynamic Range images

High dynamic range (HDR) images are characterized by a very wide intensity range that exceeds by far the range that can be displayed on conventional displays. Examples for such images can be a scene combining indoor and outdoor details, or scene with bright lights and shadows. HDR images are obtained either by advanced digital imaging systems, or synthetically by algorithms that combine several images (see [51] for such an example).

The common way to deal with this problem is to compress the intensity to a narrower range of display intensities (for example from approx. 16 bits down to less than 8 bits). Many algorithms have been presented in the literature for this purpose, and can be divided into two main categories: tone reproduction curves (TRC) and tone-reproduction-based opera-

tors (TRO). See [52] for a summary.

It is important to obsereve that such a task is curried out easily by our visual system. Natural scenes span HDR of intensities, and the neural coding bandwidth is of the same magnitude of a display or even narrower (around 6 bits [53]). For this reason, some methods such as [18], [19], [53] and [54] are inspired by the HVS and try to mimic its function in order to compress the HDR image to a LDR images. The AGC model proved to have high correlation with experimental results regarding intensity, and, as discussed earlier, one of its major characteristics is the compression of a wide dynamic rage. Therefore, it is natural to use AGC processing to compress HDR input to a narrower range, that can be displayed on a regular screen, and yet have a high sensitivity.

A LDR image (I_{LDR}) is obtained by adding a logarithmic version of the original HDR image (I_{HDR}) multiplied by attenuation constant (γ) to the response of the AGC model with I_{HDR} as the input (I_{AGC}):

$$I_{LDR} = I_{AGC} + \gamma \log(1 + I_{HDR}), \tag{28}$$

where $\gamma = 0.004$ and $W = [0.4\ 5\ 0.4]$.

Using AGC has many advantages: processing can be made in parallel over the entire image (especially when the AGC is implemented using ANN), no "halo" artifacts appear, the relative contrast is increased (the AGC compresses the "common" attributes of the stimuli while enhancing the novelty) and, in general, the human observer that looks at this image on the screen gets an image that is more "natural" for him – an image that is processed with a mechanism similar to the HVS and further enhances the natural processing. The important issue regarding the compression process is to preserve details in bright areas as well as details in the dark areas, together with the general illumination perception. This process is demonstrated by using a synthetic image (Fig. 21) and the Stanford Memorial Church HDR image (taken from Paul Debevec's home page; Fig. 22).

These results demonstrate that the proposed technique performs effectively in compressing HDR image into LDR image as required by most conventional displays. An important feature characteristic of the AGC-based processing approach is that local details are well preserved and in some cases enhanced. Comparing our method with the default Matlab function shows that the AGC-based processing performs at least equally well, and in some cases even better. A very important property of our technique is that it is completely free of halo artifacts, contrary to the Matlab function (see the dark region in Fig. 22 (a)). Moreover, the result obtained by application of the method presented herein is more realistic, yielding results more similar to what we expect to see when observing such scene.

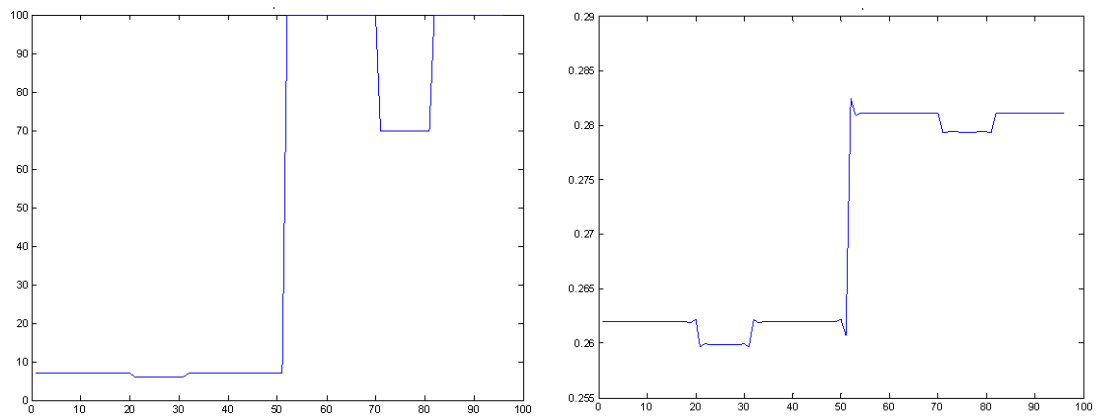

(a) (b)

Fig. 21: (a) Simple example of HDR image combining two illumination regions and details in both of them. (b) The result of the AGC algorithm. The dynamic range is compressed, while both details and illumination perception are preserved.

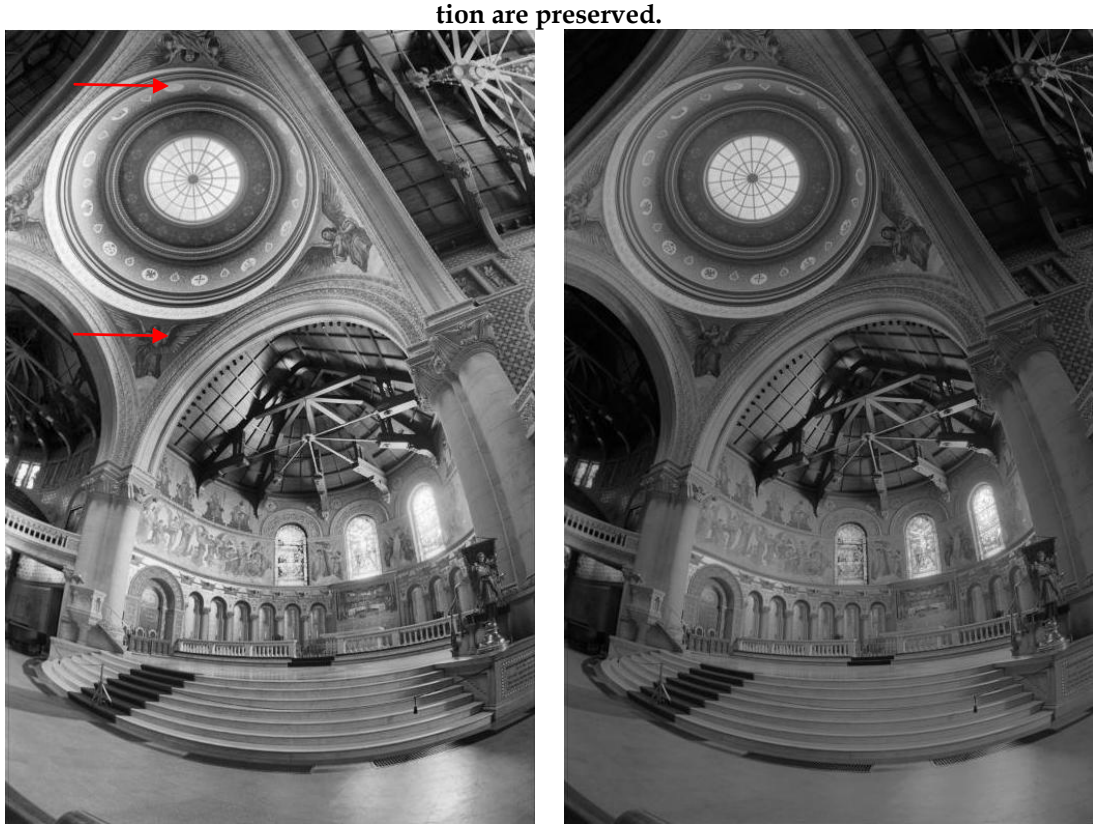

(a) (b)

Fig. 22: The Stanford Memorial Church LDR image obtained by using (a) Matlab function "tonemap", (b) AGC algorithm. This technique is completely free of halo artifacts, contrary to the Matlab function (see the dark region marked in errow in (a)). Eventhough some regions of (b) seem darker than those of (a), the result obtained by application of the method presented herein is more realistic, yielding results more similar to what we expect to see when observing such scene

4.2 Enhanced Edge Detection

An important problem in image processing is the detection of edges in a given image. A number of schemes have been proposed for this purpose [55]. These are applied as a preprocessing operation prior to high level image analysis. Edge detection is assumed to be a crucial step in the visual path, and part of the early visual processing [56].

Canny's edge detector [57] is still considered to be a good and standard edge detector for many purposes. It is based on

first order operators (discrete derivative), which produce an output that corresponds to the difference between the values of neighboring pixels. Such operators can not, however, consistently locate object boundaries in the presence of changes in scene illumination, and second order operators cannot resolve this problem [58].

An example of such a case is highlighted in Fig. 23. To overcome this limitation, we can extract the edges of an image by preprocessing with AGC. As discussed earlier, by processing an image with AGC, we get a local spatial adaptation, which diminishes the slowly varying of illumination over the global scene. In addition, the AGC processing also enhances sharp variations, thus increasing the relative contrast or slope of edges, while suppressing the noise. Moreover, the AGC is believed to model the HVS, which extracts edges much better than Canny edge detector. Therefore, applying AGC processing prior to the application of first order edge detection (such as canny's) is expected to enhance the performance of edge detection over poorly illuminated environments.

(a) (b) (c)

Fig. 23: Example of edge extraction in regions with poor illumination. (a) An image with regions of poor illumination marked by red ellipses. (b) Edges obtained by applying Canny operator. . Edges at the marked regions are not detected due to poor illumination. (c) Edges enhanced by the application of the Canny edge detector to the image preprocessed by the AGC operator. Edges at marked regions are now detected

4.3 Curve completion due to occlusion

Contour interpolation, inpainting the missing parts between two contour fragments is a ubiquitous phenomenon. Numerous objects that appear in nature images, are bounded by edges that are not fully defined by visual information. In many cases, the lack of visual specification stems from partial occlusion by surrounding objects; in other cases, incomplete edge specification arises from a lack of contrast with the background environment. Contour interpolation leads to the perception of a clearly defined object boundary even though these boundaries are missing [See Fig. 24 for some examples of this phenomenon].

A brief review on this subject can be found in [59], where the authors concluded that curve completion is an early visual process that takes place as low as at the primary visual cortex, and that the participation of early visual neurons in the representation of curves is not limited to viewable curves only, but is also extended to completed or illusory curves as well

(see also [60]). These findings suggest that contour interpolation involves basic perceptual mechanism and that real and interpolated contours are processed in parallel. Therefore, they conclude that network-style models of completion processes are most likely to be the mechanism underlying contour interpolation.

(a) (b)

Fig. 24: Examples of curve completion due to (a) lack of contrast with the background (adopted from [59]). (b) Partial occlusion (adopted from [61])

Indeed, many networks for curve completion have been introduced in the literature [62], [63]. But, even though Singh and Fulvio [64] concluded that the visual system systematically takes into account the curvature of inducing contours when extrapolating their shapes and that a successful model must take into account the curvatures, all of them use array of cells selective for orientation.

Kimia et al. [61] motivated by railroad design methods of the early 1900's, which connects two rail segments by "transition curves", proposed the minimization of an energy functional that penalizes changes in curvature as a completion model, i.e. minimizing the following:

$$\int \left(\frac{d\kappa}{ds} \right)^2 ds \,. \tag{29}$$

This kind of minimization immediately entails a linear expression for the curvature as a function of the arc length, a class of curves known as Euler Spirals. Although this model satisfies all the axioms mentioned in [59], it fails to predict some experiments results [64], since the interpolated curvature should decrease asymptotically to zero if no end segment exists (i.e. the curve is extrapolated from only one segment), and a nonlinear decrease in the curvature fits better the results than a linear decrease.

Based on the above insights, and motivated by our model of the HVS, we propose a novel model for curve completion that combines both the AGC and the Euler Spirals in a network-style model. The idea is that the curve completion is performed along the curvature dimension. The missing curvature data of the curve is linearly interpolated between the curvature value of the first segment to the curvature value of the second segment. The interpolated curve is then entered as an input to the AGC network. The response of the system is the perceived curve. If only one segment exists, the second segment is referred to as a zero curvature segment. In this way the extrapolated curve has a nonlinear decrease in its curvature as suggested above. Moreover, this model can explain the "cost of curvature" [64], and scale-dependency [65], [66], of

the interpolated curves.

The "cost of curvature" means that the precision with which an interpolated contour is represented becomes systematically weaker with increasing curvature. This is interpreted in the context of the AGC model according to the small signal analysis as follows: when the input intensity is higher (e.g. the curvature increases), the sensitivity of the system decreases.

Scale-dependency means that the interpolation depends on the viewing distance. This is an obvious outcome for interpolating the curve along the curvature dimension. The curvature depends on the curve radius, and the radius, in turn, is a function of the viewing distance.

The model is tested on a few simple curves to demonstrate the main ideas. For each curve an occlusion is simulated by removing part of the curvature information. The missing curvature values are then linearly interpolated between the last curvature value of the first segment to the first curvature value of the second segment. The interpolated curvature values serve as input to the AGC model and the response is referred to as the interpolated curve. The parameters of the AGC are: $W(x) = 1/[length\ of\ W]$, with W extending across 11 pixels.

Fig. 25 depicts the result of completion of a curve with constant curvature (i.e. part of a circle). As this example may look very simple and worthless, one should keep in mind that this result is simple only because the curve is interpolated along the curvature dimension. If, for example, the curve would have been interpolated along the tangent dimension the problem would become more complicated. Fig. 26 depicts the result of curve completion for the case when only one segment is present. Note how the curvature values decrease to zero (as noted in [64]). Fig. 27 depicts curve completion when a sudden and abrupt change in curvature occurs. Part of the curve consists of some constant curvature value, while the other part consists of the same constant curvature but of opposite sign. When the occluded portion increases in length, the interpolated curve becomes smoother, and the changes comparing to the original curve are much more noticeable. Nevertheless, one should keep in mind that the interpolated curve should not be compared to the original curve but to the curve that a human observer will perceive. Fig. 27 (e) looks "pleasing", and it seems that a human observer will draw such smooth curve given the occluded curve.

5 Discussion and Conclusions

BIOLOGICAL and man-made visual systems, alike, are concerned with detection and enhancement of novel events. Novelty is associated with the unexpected that cannot, for example, be linearly predicted. Qualitative speaking, important and interesting 'events' along image contours, for example, consist primarily of abrupt changes in orientation and curvature, as is the case with other image attributes (dimensions). Local maxima of curvature, and inflection points (i.e. zero crossings of curvature) identify in this case such events (see [67], [68], [69] and [70]). This fact is well known by artists and

cartoonists who exploit it in their artwork, as much as they do, and in more familiar manner, with regard to other image attributes such as intensity and color. Moreover, zero crossings of curvature can be the basis of shape representation for planar curves [71]. Similarly to biological visual systems that emphasize changes and adapt to locally-constant values of the image attributes, this is indeed an important feature of curvature processing (or of processing of other image attributes) by adaptive computer vision and image processing systems endowed with the mechanism/algorithm of AGC. Curvature emphasis and adaptation (see Fig. 12 and Fig. 13) occur simultaneously and their extent can be controlled by adjusting the parameter k of the "hardwired" processor connectivity.

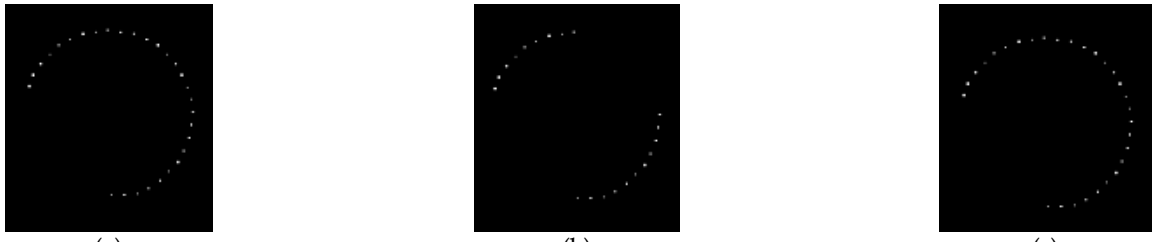

(a) (b) (c)

Fig. 25: Simulation result for interpolating curve with a constant curvature. (a) Original curve. (b) The occluded curve. (c) The interpolated curve. The occluded segment is a linear combination of the contour fragments and, thus, (c) is identical to (a).

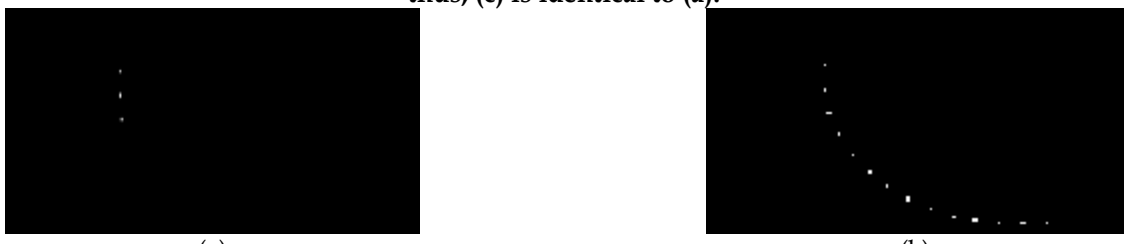

(a) (b)

Fig. 26: Simulation result for interpolating curve with only one segment. (a) The given segment. (b) The interpolated curve.

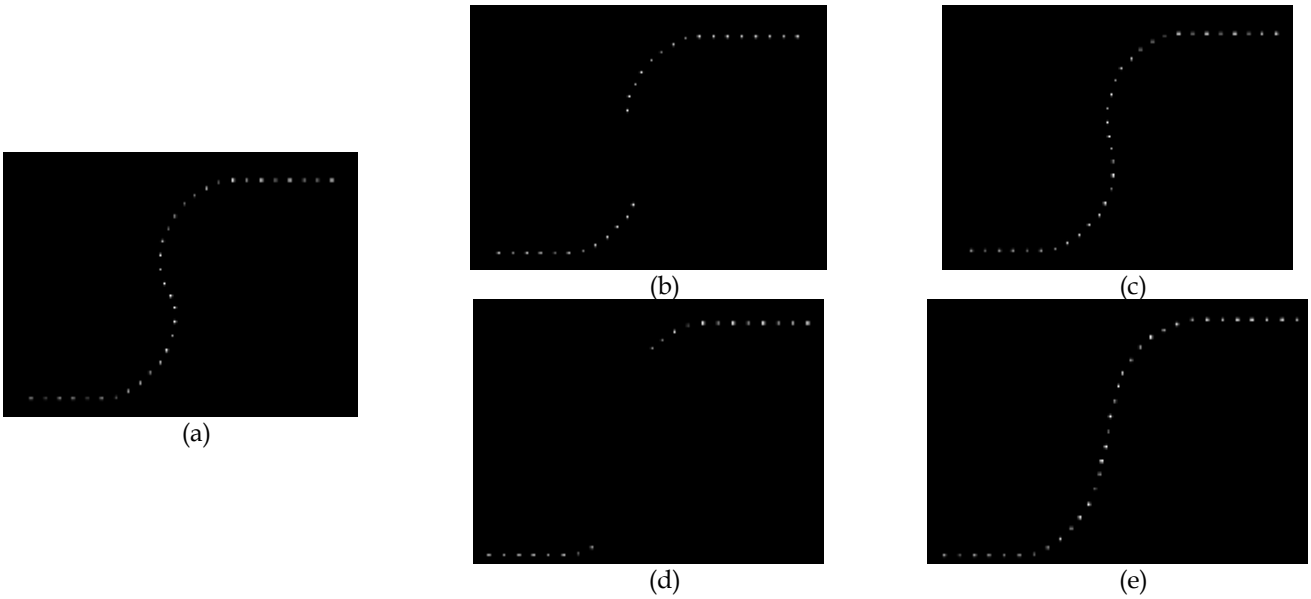

(a) (b) (c) (d) (e)

Fig. 27: Simulation result for interpolating curve with an abrupt change in curvature. (a) Original curve. (b) The occluded curve. (c) The interpolated curve of (b). (d) A curve with a longer occluded region. (e) The interpolated curve of (d). The occluded part is where the abrupt change in curvature occurs and thus (c) and (e) are only a smooth version of (a). The occluded part in (b) is small and therefore the changes in (c) are almost unnoticeable. The occluded part in (d) is large and therefore the changes between (a) and (e) are quite significant but, neverthe-

less, (e) looks like a "pleasing" continuous curve to the human observer.

Inspecting the results of size processing indicates a good correspondence between the adaptive system response (Fig. 16) and the psychophysical experimental results (Fig. 10), for both the distance and size parameters. Such results are expected in view of the dependency of AGC on these two parameters as well, i.e. cells proximity and specificity (in this case, objects' size).

Inspecting the results of depth processing, indicates a good correspondence between the adaptive system response (Fig. 19) and the psychophysical experimental results (Fig. 11). Moreover, these results can be understood also from the aspect of convex-concave adaptation (Fig. 20). This leads to the conclusion that depth adaptation may be explained by curvature adaptation (and maybe adaptation of other dimensions) or vice versa.

Understanding the HVS and modeling its characteristics by an adaptive system is of a considerable interest because of its potential implementation in the design of intelligent computer vision and image processing algorithms and systems. Because of the complexity of the processes involved, and in order to account for the vast volume of available experimental data, there is a need for relatively simple models. As shown, the generalized AGC system is relatively simple (only few parameters) and versatile. It does not call for postulating any components of neural circuitry more complex than those well known to exist in biological neural networks and, yet, shows good correlation with psychophysical experiments. Such understanding is crucial now that visual prosthetics are becoming a workable reality. These visual prosthetics use different medical and technical approaches such as stimulating the visual cortex or even the retina [2] [72]. In all these studies, the subjects had to be trained for recognizing and discriminating different patterns of simulations [73]. The main concern of these studies is whether the subject can have a visual perception and what are the proper stimulus parameters. None of them consider, however, the important question of what is the optimal stimulus, i.e. how should the computing elements (neurons) be stimulated in order to achieve the best visual perception of a given image (or the shortest necessary training period). Such optimal stimulation may be based on our understanding of the visual system, as presented, for example, within this work.

Implementing the AGC model on all image elementary features (dimensions), or other modalities for this matter, provides great advantages. It constitutes a universal and parsimonious model that explains how our visual system processes visual information along its various dimensions, before the later stage of sequential "visual routines" is implemented. Such mechanism can process an image along all its dimensions (that are yet to be defined). The only necessary information is the relevant projections (detectors). Further, it may lead to the development of a metric for distance between images, and it can be instrumental in performing important tasks, such as recognition and classification. Such computer vision tasks can be executed along the different feature dimensions and be further mapped nonlinearly without recombination of

the separate processed feature maps back onto an image.

The AGC model elucidates the ability of our HVS to span HDR of inputs along various dimensions, while still having high sensitivity. This ability has been well known and investigated with reference to the intensity dimension. Here we have shown how powerful it can be along other dimensions. For example, it highlights how can we see curve with curvature values that vary from infinity (straight lines) to almost zero (the limit is defined only by the retina resolution), and yet notice differences between curves in the order of 10^{-5} (see [74] and [75] for more details). This interpretation is valid also for depth perception (see [76] and [77] for more details), size, texture, orientation, motion and more.

It appears as though the AGC mechanism repeats itself along all stages of sensory processing in the CNS [78], [79] and [80], in order to remove statistical redundancy [17]. Therefore, having this model allows us to mimic the HVS (or other sensory modalities), and to propose a unified model for biological sensory processing.

Likewise this model allows us also to process an image not only in the intensity/spatio-temporal domain, but also along all other visually-important dimensions. For example, in the case of a given a noisy curve, one can further reduce the noise along the curvature dimension (in addition to the AGC-based noise reduction) with standard filters, such as non-linear diffusion filter. As discussed above, one can also overcome occlusions by interpolating along the curvature dimension and create HDR images, or enhance edge detection processing along the intensity dimension.

The proposed visual AGC mechanism can enhance existing schemes of intelligent image processing with reference to enhancement of various image attributes and features, i.e. curvature, size and other image attributes.

The projection and decomposition of an image into its intrinsic dimensions is by no means the only possible model of representation and processing of images, and definitely not always the optimal one. Within this work we considered the different image dimensions independent of each other. This, of course, should be further analyzed, as more image dimensions should be considered, and, obviously, the independency assumption is not always valid. An alternative approach, introduced in the context of image processing and computer vision [81], [82], considers an image to be a manifold embedded in higher dimensional combined position (spatial)-feature space. The features are then the image attributes or dimensions, such as color, curvature and size mentioned above. Adaptation by means of nonlinear gain control is executed in this case in the multidimensional space in a unified manner. Such manifolds are yet to be further investigated.

APPENDIX A – SNR CALCULATIONS FOR THE AGC MODEL

An analytic solution for the SNR of the step response, according to the definition of (20) can be obtained by using the input-output noise variance relations as in (14) or (19) and the analytic step response of the AGC model given by [10]. For convenience, all equations are rewritten here using the notations of this paper. In this case, the input is:

$$s(x) = a_1 + a_2 U(x), \tag{30}$$

where a_1 is the lower constant intensity on the LHS of the step and a_2 is the difference between the intensity on the RHS

and on the LHS. The contrast of the input is defined by (21), and is given by:

$$\tilde{C}_{m,s} = \frac{a_2}{2a_1 + a_2}. \tag{31}$$

When the feedback kernel is an exponential:

$$W(x) = k\frac{\gamma}{2}e^{-\gamma|x|}, \tag{32}$$

the response is given by:

$$r(x) = \begin{cases} \dfrac{a_1}{1+ka_1}\left(1 - \dfrac{ka_2}{\left(1+\sqrt{\dfrac{1+ka_1}{1+k(a_1+a_2)}}\right)\left[1+k(a_1+a_2)\right]}e^{\gamma\sqrt{1+ka_1}x}\right) & , x<0 \\ \dfrac{a_1+a_2}{1+k(a_1+a_2)}\left(1 + \dfrac{ka_2}{\left(1+\sqrt{\dfrac{1+k(a_1+a_2)}{1+ka_1}}\right)(1+ka_1)}e^{-\gamma\sqrt{1+k(a_1+a_2)}x}\right) & , x>0 \end{cases}. \tag{33}$$

For calculating the contrast, only the minimum and maximum values of the response are relevant and are obtained by:

$$\begin{aligned} MIN\{r(x)\} &= \frac{a_1}{1+ka_1}\left(1 - \frac{ka_2}{\left(1+\sqrt{\dfrac{1+ka_1}{1+k(a_1+a_2)}}\right)\left[1+k(a_1+a_2)\right]}\right) \\ MAX\{r(x)\} &= \frac{a_1+a_2}{1+k(a_1+a_2)}\left(1 + \frac{ka_2}{\left(1+\sqrt{\dfrac{1+k(a_1+a_2)}{1+ka_1}}\right)(1+ka_1)}\right) \end{aligned}. \tag{34}$$

The contrast is defined by (21):

$$\tilde{C}_m = \frac{MAX\{r(x)\} - MIN\{r(x)\}}{MAX\{r(x)\} + MIN\{r(x)\}}. \tag{35}$$

Substituting (34) in (35) yields:

$$\tilde{C}_{m,r} = \frac{a_2}{2a_1 + a_2}. \tag{36}$$

Comparing (31) to (36) reveals the fact that the contrast of the input is equal to the contrast of the output! Therefore, the SNR improvement is given by:

$$\frac{SNR_r}{SNR_s} = \frac{\tilde{C}_{m,r}^{\,2}}{\sigma_r^{\,2}} \cdot \frac{\sigma_s^{\,2}}{\tilde{C}_{m,s}^{\,2}} = \frac{\sigma_s^{\,2}}{\sigma_r^{\,2}}. \tag{37}$$

Substituting (14) in (37) yields:

$$\frac{SNR_r}{SNR_s} = \left(\frac{1+a_1+a_2}{\alpha}\right)^2 \; or \; \left(\frac{1+a_1}{\alpha}\right)^2, \tag{38}$$

where the two options depende on the choice of the variance used (i.e. the noise at the upper part or lower part of the step, respectively).

REFERENCES

[1] Jiawei Yang et al., "A super low power MICS band receiver in 65 nm CMOS for high resolution epi-retinal prosthesis," pp. 435-438, Oct. 2009.

[2] N. Tran et al., "A fully flexible stimulator using 65 nm cmos process for 1024-electrode epi-retinal prosthesis," pp. 1643-1646, Sep. 2009.

[3] C. Koch, W. Mokwa, M. Goertz, and P. Walter, "First results of a study on a completely implanted retinal prosthesis in blind humans," pp. 1237-1240, Oct. 2008.

[4] Y. Y. Zeevi and E. R. Kronauer, "Reorganization and diversification of signals in vision," *EEE transactions on systems, man, and cybernetics*,

vol. 15, no. 1, pp. 91-101, 1985.
[5] D. H. Hubel and T. N. Wiesel, "Brain mechanisms of vision," *Scientific American*, vol. 241, no. 3, pp. 150-162, Sep. 1979.
[6] J. J. Gibson, "Adaptation with negative after-effect.," *Psychological Review*, vol. 44, no. 3, pp. 222-244, 1937.
[7] Y. Y. Zeevi and S. S. Mangoubi, "Noise suppression in photoreceptors and its relevance to incremental intensity thresholds," *Journal of the Optical Society of America*, vol. 68, no. 12, pp. 1772-1776, Dec. 1978.
[8] M. J. Wainwright, "Visual adaptation as optimal information transmission," *Vision Research*, vol. 39, no. 23, pp. 3960-3974, Nov. 1999.
[9] S. Ullman and G. Schechtman, "Adaptation and Gain Normalization," *Proceedings of the Royal Society of London. Series B. Biological Sciences*, vol. 216, no. 1204, pp. 299-313, Oct. 1982.
[10] Y. Y. Zeevi and M. Shefer, "Automatic gain control of signal processing in vision," *Journal of the Optical Society of America*, vol. 71, p. 1556.
[11] Y. Weltsch-Cohen, "AGC models for signal processing in the primary visual cortex," M.Sc. Thesis, Technion, 2002.
[12] J. Ding and G. Sperling, "A gain-control theory of binocular combination," *Proceedings of the National Academy of Sciences of the United States of America*, vol. 103, no. 4, pp. 1141-1146, Jan. 2006.
[13] Z. L. Lu and G. Sperling, "Contrast gain control in first- and second-order motion perception," *Journal of the Optical Society of America A*, vol. 13, no. 12, pp. 2305-2318, Dec. 1996.
[14] J. J. Du Croz and W. A. H. Rushton, "The separation of cone mechanisms in dark adaptation," *The Journal of Physiology*, vol. 183, no. 2, pp. 481-496, Mar. 1966.
[15] J. Krauskopf and J. D. Mollon, "The independence of the temporal integration properties of individual chromatic mechanisms in the human eye," *The Journal of Physiology*, vol. 219, no. 3, pp. 611-623, Dec. 1971.
[16] R. Shapley and C. ENROTH-CUGELL, "Visual adaptation and retinal gain controls," *Progress in retinal research*, vol. 3, pp. 263-346, 1984.
[17] O. Schwartz and E. P. Simoncelli, "Natural signal statistics and sensory gain control," *Nat Neurosci*, vol. 4, no. 8, pp. 819-825, 2001.
[18] R. Ginosar, O. Hilsenrath, and Y. Y. Zeevi, "United States Patent: 5144442 - Wide dynamic range camera," U.S. Patent 514444201-Sep-1992.
[19] Y. Y. Zeevi, R. Ginosar, and O. Hilsenrath, "United States Patent: 5420637 - Dynamic image representation system," U.S. Patent 542063730-May-1995.
[20] J. Ohlson, "Exact Dynamics of Automatic Gain Control," *Communications, IEEE Transactions on*, vol. 22, no. 1, pp. 72-75, 1974.
[21] H. P. Snippe and J. H. Hateren, "Dynamics of Nonlinear Feedback Control," *Neural Computation*, vol. 19, no. 5, pp. 1179-1214, May. 2007.
[22] L. D. Griffin, M. Lillholm, and M. Nielsen, "Natural image profiles are most likely to be step edges," *Vision Research*, vol. 44, no. 4, pp. 407-421, Feb. 2004.
[23] F. Ratliff, "Mach bands: Quantitative studies on neural networks in the retina," *Holden-Day inc.*, 1965.
[24] S. S. Mangoubi, "Noise and thresholds in vision," PHD. Thesis, Technion, 1979.
[25] A. A. Faisal, L. P. J. Selen, and D. M. Wolpert, "Noise in the nervous system," *Nature reviews. Neuroscience*, vol. 9, no. 4, pp. 292-303, Apr. 2008.
[26] A. Papoulis, *Probability, Random Variables and Stochastic Processes*, 1st ed. McGraw-Hill Companies, 1965.
[27] M. Carmo, *Differential geometry of curves and surfaces*. Upper Saddle River N.J.: Prentice-Hall, 1976.
[28] S. Hochstein and M. Ahissar, "View from the top: hierarchies and reverse hierarchies in the visual system," *Neuron*, vol. 36, no. 5, pp. 791-804, Dec. 2002.
[29] P. Cavanagh, M. Arguin, and A. Treisman, "Effect of surface medium on visual search for orientation and size features.," *Journal of Experimental Psychology: Human Perception and Performance*, vol. 16, no. 3, pp. 479-491, 1990.
[30] J. M. Wolfe, S. J. Butcher, C. Lee, and M. Hyle, "Changing your mind: On the contributions of top-down and bottom-up guidance in visual search for feature singletons.," *Journal of Experimental Psychology: Human Perception and Performance*, vol. 29, no. 2, pp. 483-502, 2003.
[31] A. M. Treisman and S. Gormican, "Feature analysis in early vision: Evidence from search asymmetries.," *Psychological Review*, vol. 95, no. 1, pp. 15-48, 1988.
[32] J. T. Enns and R. A. Rensink, "Influence of scene-based properties on visual search," *Science (New York, N.Y.)*, vol. 247, no. 4943, pp. 721-723, Feb. 1990.
[33] J. T. Enns and R. A. Rensink, "Sensitivity to Three-Dimensional Orientation in Visual Search," *Psychological Science*, vol. 1, no. 5, pp. 323-326, 1990.
[34] M. Coltheart, "Visual feature-analyzers and aftereffects of tilt and curvature.," *Psychological Review*, vol. 78, no. 2, pp. 114-121, 1971.
[35] S. Hancock and J. W. Peirce, "Selective mechanisms for simple contours revealed by compound adaptation," *Journal of Vision*, vol. 8, no. 7, pp. 1-10, Jun. 2008.
[36] L. A. Riggs, "Curvature as a Feature of Pattern Vision," *Science*, vol. 181, no. 4104, pp. 1070-1072, Sep. 1973.
[37] C. F. Stromeyer and L. A. Riggs, "Curvature Detectors in Human Vision?," *Science*, vol. 184, no. 4142, pp. 1199-1201, Jun. 1974.
[38] J. J. Koenderink and A. J. V. Doorn, "Representation of local geometry in the visual system," *Biological Cybernetics*, vol. 55, no. 6, pp. 367-375, Mar. 1987.
[39] A. Dobbins, S. W. Zucker, and M. S. Cynader, "Endstopped neurons in the visual cortex as a substrate for calculating curvature," *Nature*, vol. 329, pp. 438-441, Oct. 1987.
[40] H. R. Wilson, F. Wilkinson, and W. Asaad, "Concentric orientation summation in human form vision," *Vision Research*, vol. 37, no. 17, pp. 2325-2330, Sep. 1997.
[41] N. S. Sutherland, "Outlines of a Theory of Visual Pattern Recognition in Animals and Man," *Proceedings of the Royal Society of London. Series B, Biological Sciences*, vol. 171, no. 1024, pp. 297-317, Dec. 1968.
[42] C. Blakemore and F. W. Campbell, "On the existence of neurones in the human visual system selectively sensitive to the orientation and size of retinal images," *The Journal of Physiology*, vol. 203, no. 1, pp. 237-260.1, Jul. 1969.
[43] D. P. Carey, M. Harvey, and A. D. Milner, "Visuomotor sensitivity for shape and orientation in a patient with visual form agnosia," *Neuropsychologia*, vol. 34, no. 5, pp. 329-337, May. 1996.
[44] D. H. Hubel and T. N. Wiesel, "Stereoscopic Vision in Macaque Monkey: Cells sensitive to Binocular Depth in Area 18 of the Macaque Monkey Cortex," *Nature*, vol. 225, pp. 41-42, Jan. 1970.
[45] W. CURRAN and A. JOHNSTON, "Three-dimensional Curvature Contrast--Geometric or Brightness Illusion?," *Vision Research*, vol. 36, no. 22, pp. 3641-3653, Nov. 1996.
[46] M. Graham and B. J. Rogers, "Simultaneous and successive contrast effects in the perception of depth from motion-parallax and stereoscopic information," *Perception*, vol. 11, no. 3, pp. 247 – 262, 1982.
[47] D. H. Hubel and T. N. Wiesel, "Receptive fields and functional architecture of monkey striate cortex," *The Journal of Physiology*, vol. 195, no. 1, pp. 215-243, Mar. 1968.

[48] B. Roberts, M. G. Harris, and T. A. Yates, "The roles of inducer size and distance in the Ebbinghaus illusion (Titchener circles)," *Perception*, vol. 34, no. 7, pp. 847 – 856, 2005.
[49] P. Parent and S. W. Zucker, "Trace Inference, Curvature Consistency, and Curve Detection," *IEEE Transactions on Pattern Analysis and Machine Intelligence*, vol. 11, no. 8, pp. 823-839, 1989.
[50] S. W. Zucker, C. David, A. Dobbins, and L. Iverson, "The Organization Of Curve Detection: Coarse Tangent Fields And Fine Spline Coverings," presented at the Computer Vision., Second International Conference, 1988, pp. 568-577.
[51] P. E. Debevec and J. Malik, "Recovering high dynamic range radiance maps from photographs," in *ACM SIGGRAPH 2008 classes*, Los Angeles, California, 2008, pp. 1-10.
[52] M. Herscovitz and O. Yadid-Pecht, "A modified Multi Scale Retinex algorithm with an improved global impressionof brightness for wide dynamic range pictures," *Machine Vision and Applications*, vol. 15, no. 4, pp. 220-228, Oct. 2004.
[53] V. Brajovic, "Brightness perception, dynamic range and noise: a unifying model for adaptive image sensors," in *Computer Vision and Pattern Recognition, 2004. CVPR 2004. Proceedings of the 2004 IEEE Computer Society Conference on*, 2004, vol. 2, p. II-189-II-196 Vol.2.
[54] T. Tanaka and N. Ohnishi, "Painting-like Image Emphasis based on Human Vision Systems," *Computer Graphics Forum*, vol. 16, no. 3, p. C253-C260, 1997.
[55] T. Peli and D. Malah, "A study of edge detection algorithms," *Computer Graphics and Image Processing*, vol. 20, no. 1, pp. 1-21, Sep. 1982.
[56] D. Marr and E. Hildreth, "Theory of Edge Detection," *Proceedings of the Royal Society of London. Series B. Biological Sciences*, vol. 207, no. 1167, pp. 187-217, Feb. 1980.
[57] J. Canny, "A Computational Approach to Edge Detection," *IEEE Transactions on Pattern Analysis and Machine Intelligence*, vol. 8, no. 6, pp. 679-698, Nov. 1986.
[58] R. P. Johnson, "Contrast based edge detection," *Pattern Recognition*, vol. 23, no. 3-4, pp. 311-318, 1990.
[59] G. Ben-Yosef and O. Ben-Shahar, "Minimum length in the tangent bundle as a model for curve completion," in *Computer Vision and Pattern Recognition (CVPR), 2010 IEEE Conference on*, 2010, pp. 2384-2391.
[60] S. E. Guttman and P. J. Kellman, "Contour interpolation revealed by a dot localization paradigm," *Vision Research*, vol. 44, no. 15, pp. 1799-1815, Jul. 2004.
[61] B. Kimia, I. Frankel, and A. M. Popescu, "Euler Spiral for Shape Completion," *International Journal of Computer Vision*, vol. 54, no. 1, pp. 159-182, Aug. 2003.
[62] S.-C. Yen and L. H. Finkel, "Extraction of perceptually salient contours by striate cortical networks," *Vision Research*, vol. 38, no. 5, pp. 719-741, Mar. 1998.
[63] D. J. Field, A. Hayes, and R. F. Hess, "Contour integration by the human visual system: Evidence for a local 'association field'," *Vision Research*, vol. 33, no. 2, pp. 173-193, Jan. 1993.
[64] M. Singh and J. M. Fulvio, "Visual extrapolation of contour geometry," *Proceedings of the National Academy of Sciences of the United States of America*, vol. 102, no. 3, pp. 939 -944, Jan. 2005.
[65] C. Fantoni and W. Gerbino, "Contour interpolation by vector-field combination," *Journal of Vision*, vol. 3, no. 4, May. 2003.
[66] W. Gerbino and C. Fantoni, "Visual interpolation is not scale invariant," *Vision Research*, vol. 46, no. 19, pp. 3142-3159, Oct. 2006.
[67] D. D. Hoffman and W. A. Richards, "Parts of recognition," *Cognition*, vol. 18, no. 1-3, pp. 65-96, Dec. 1984.
[68] J. J. Koenderink and A. J. V. Doorn, "The shape of smooth objects and the way contours end," *Perception*, vol. 11, no. 2, pp. 129 – 137, 1982.
[69] W. Richards, B. Dawson, and D. Whittington, "Encoding contour shape by curvature extrema," *Journal of the Optical Society of America A*, vol. 3, no. 9, pp. 1483-1491, 1986.
[70] M. A. Fischler and R. C. Bolles, "Perceptual organization and curve partitioning," *IEEE Trans. Pattern Anal. Mach. Intell.*, vol. 8, no. 1, pp. 100-105, 1986.
[71] F. Mokhtarian and A. K. Mackworth, "A theory of multiscale, curvature-based shape representation for planar curves," *Pattern Analysis and Machine Intelligence, IEEE Transactions on*, vol. 14, no. 8, pp. 789-805, 1992.
[72] W. H. Dobelle, "Artificial vision for the blind by connecting a television camera to the visual cortex," *ASAIO Journal (American Society for Artificial Internal Organs: 1992)*, vol. 46, no. 1, pp. 3-9, Feb. 2000.
[73] M. S. Humayun et al., "Visual perception in a blind subject with a chronic microelectronic retinal prosthesis," *Vision Research*, vol. 43, no. 24, pp. 2573-2581, Nov. 2003.
[74] R. J. Watt and D. P. Andrews, "Contour curvature analysis: Hyperacuities in the discrimination of detailed shape," *Vision Research*, vol. 22, no. 4, pp. 449-460, 1982.
[75] R. J. Watt, "Further evidence concerning the analysis of curvature in human foveal vision," *Vision Research*, vol. 24, no. 3, pp. 251-253, 1984.
[76] S. B. Kaye et al., "Monocular and Binocular Depth Discrimination Thresholds," *Optometry & Vision Science*, vol. 76, no. 11, 1999.
[77] T. Kumar and D. A. Glaser, "Depth discrimination of a line is improved by adding other nearby lines," *Vision Research*, vol. 32, no. 9, pp. 1667-1676, Sep. 1992.
[78] L. F. Abbott, J. A. Varela, K. Sen, and S. B. Nelson, "Synaptic Depression and Cortical Gain Control," *Science*, vol. 275, no. 5297, pp. 221-224, Jan. 1997.
[79] E. Salinas, "Gain Modulation: A Major Computational Principle of the Central Nervous System," *Neuron*, vol. 27, no. 1, pp. 15-21, Jul. 2000.
[80] Y. F. Sit, Y. Chen, W. S. Geisler, R. Miikkulainen, and E. Seidemann, "Complex Dynamics of V1 Population Responses Explained by a Simple Gain-Control Model," *Neuron*, vol. 64, no. 6, pp. 943-956, Dec. 2009.
[81] R. Kimmel, R. Malladi, and N. Sochen, "Images as Embedded Maps and Minimal Surfaces: Movies, Color, Texture, and Volumetric Medical Images," *International Journal of Computer Vision*, vol. 39, no. 2, pp. 111-129, 2000.
[82] N. Sochen and Y. Y. Zeevi, "images as manifolds embedded in a spatial feature non euclidean space," *IEEE ICIP*, pp. 166-170, 1998.